

Exosomal circRNA FNDC3B promotes the progression of esophageal squamous cell carcinoma by sponging miR-490-5p and regulating thioredoxin reductase 1 expression

Bo Tang, Qingfeng Zhang, Kui Liu, and Yun Huang

Department of Cardio-Thoracic Surgery, Zigong Fourth People's Hospital, Zigong City, China

ABSTRACT

Exosomal circular RNAs (circRNAs) have been reported to play critical roles in esophageal squamous cell carcinoma (ESCC). We aimed to investigate the function of exosomal circRNA FNDC3B (circFNDC3B). The RNA levels and protein levels were examined using RT-qPCR and western blot (WB) assays. Colony formation and EdU assays were used to assess cell proliferative ability. Cell migratory and invasive abilities were detected by wound healing and transwell assays. Cell apoptosis was measured by flow cytometry. Glycolysis was measured using commercial kits. Transmission electron microscopy (TEM) and nanoparticle tracking analysis (NTA) were applied to examine the morphology and size of exosomes. Dual-luciferase reporter, RIP and RNA pull-down assays assessed the interaction of miR-490-5p with circFNDC3B or thioredoxin reductase 1 (TXNRD1). Xenograft tumor model determined the role of exosomal circFNDC3B *in vivo*. We observed that circFNDC3B was upregulated in ESCC samples and cells, as well as ESCC-derived exosomes. CircFNDC3B could be delivered via exosomes in tumor cells, and the colony formation, proliferation, migration, invasion, glycolysis, and *in vivo* growth ability of recipient cells were weakened after co-incubation with exosomal circFNDC3B-knockdown donor cells. CircFNDC3B was a miR-490-5p sponge, and miR-490-5p inhibition reversed the role of exosomal circFNDC3B-downregulating in ESCC cells. TXNRD1 was a miR-490-5p target, and TXNRD1 elevation weakened the anti-cancer function of miR-490-5p upregulation in ESCC cells. CircFNDC3B mediated TXNRD1 expression by interacting with miR-490-5p. In conclusion, exosomal circFNDC3B drove ESCC progression via regulating the miR-490-5p/TXNRD1 axis.

Abbreviations

EC: esophageal cancer; ESCC: esophageal squamous cell carcinoma; circRNA: circular RNA; WB: western blot; TEM: transmission electron microscopy; NTA: nanoparticle tracking analysis; TXNRD1: thioredoxin reductase 1; IHC: immunohistochemistry; RT-qPCR: reverse transcription-polymerase quantitative chain reaction; GLUT1: glucose transport protein type 1; LDHA: lactate dehydrogenase A

ARTICLE HISTORY

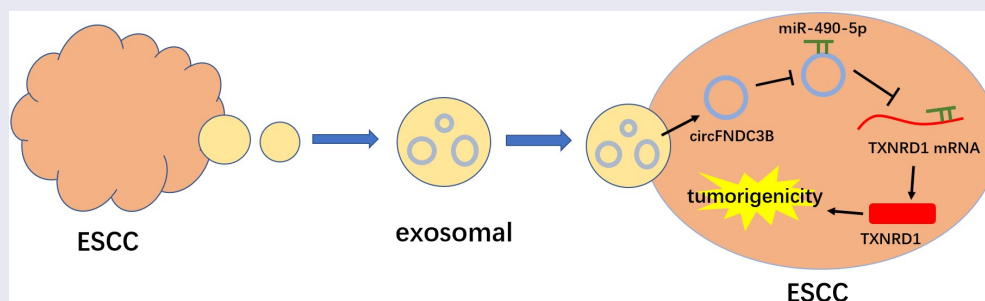
Received 11 March 2022



Revised 26 May 2022


Accepted 27 May 2022

KEYWORDS

Esophageal squamous cell carcinoma; exosome; circFNDC3B; miR-490-5p; TXNRD1



CONTACT Yun Huang  haiguai54@126.com  Department of Cardio-Thoracic Surgery, Zigong Fourth People's Hospital, No. 2, Tanmulin Street, Ziliujing District, Zigong City, Sichuan Province 643000, China

 Supplemental data for this article can be accessed online at <https://doi.org/10.1080/21655979.2022.2084484>

© 2022 The Author(s). Published by Informa UK Limited, trading as Taylor & Francis Group.

This is an Open Access article distributed under the terms of the Creative Commons Attribution-NonCommercial License (<http://creativecommons.org/licenses/by-nc/4.0/>), which permits unrestricted non-commercial use, distribution, and reproduction in any medium, provided the original work is properly cited.

Highlights

- CircFNDC3B was upregulated in ESCC samples and ESCC cell-derived exosomes.
- CircFNDC3B could be delivered via exosomes in tumor cells.
- Exosomal circFNDC3B promoted cell malignancy and glycolysis in ESCC.
- CircFNDC3B mediated TXNRD1 expression by interacting with miR-490-5p.

Introduction

Esophageal cancer (EC) is a common tumor in the world, which ranks 6th in mortality and 7th in incidence [1,2]. Esophageal squamous cell carcinoma (ESCC) is the main subtype of EC and is prevalent in China [3]. Although tremendous efforts have been made in clinical therapy, the 5-year survival rate for ESCC patients remains poor due to metastasis and recurrence [4,5]. Hence, novel biomarkers need to be identified to improve the treatment of ESCC.

CircRNAs are a special of noncoding RNAs (ncRNAs) that are generated by pre-mRNA back and characterized by conservative evolution, tissue-specific, and stable structure [6]. CircRNAs can avoid degradation by RNases and have higher stability due to their circular structures [7]. CircRNAs have drawn great attention for their involvement in the development of human cancers [8]. Many studies have studied that circRNAs are stably present in exosomes, and exosomal circRNAs are able to act as messengers of intercellular communication, thereby modulating the biological functions of target cells [9]. Exosomes originate from endosomal multivesicular bodies with a diameter of 50–140 nm [10]. Exosomes can deliver their cargo, such as circRNAs, proteins, microRNAs (miRNAs), mRNAs, or other bioactive substances to mediate the cellular communications in cancer [11,12]. Exosomal circRNAs have been reported to have potential applications as new therapeutic targets and disease biomarkers [13]. A previous report showed that circRNA_{FNDC3B} (circFNDC3B; also known as hsa_circ_0006948) was remarkably upregulated in ESCC and facilitated the development of ESCC [14]. Nevertheless, the

exact function and mechanism of exosomal circFNDC3B in ESCC are largely unknown.

According to the competitive endogenous RNA (ceRNA) networks hypothesis, circRNAs are rich in microRNA (miRNA)-binding sequence and competitively bind to miRNA response elements to function as miRNA sponges, thereby repressing miRNA activity and positively modulating the expression of target genes [15,16]. MiRNAs control protein production through binding to 3'UTR of target mRNAs, which causes mRNA degradation or inhibition of translation [17,18]. Existing evidence shows that the circRNA/miRNA/mRNA regulatory network plays an important role in EC tumorigenesis [19]. For example, circ-0000277 increased LAMA1 expression by sequestering miR-4766-5p, causing in promoting EC progression [20]. Another example was that circNTRK2 mediated ESCC cell proliferation and invasion by interacting with miR-140-3p and regulating the expression of NRIP1 [21]. Previous research has proven that miR-490-5p played a tumor-suppressing role in ESCC [22]. In this study, we found that circFNDC3B may interact with miR-490-5p, however, whether circFNDC3B can act as a sponge molecule for miR-490-5p is unclear. Thioredoxin reductase 1 (TXNRD1) acts as a tumor promoter in ESCC [23]. TXNRD1 has been predicted to be a downstream target of miR-490-5p, but whether miR-490-5p can target TXNRD1 to affect ESCC remains poorly documented.

Accordingly, the research aimed to study whether exosomal circFNDC3B is implicated in the malignancy and glycolysis of ESCC cells. In this paper, we examined circFNDC3B expression in ESCC tissue specimens and cell lines. In addition, we determined the effect of exosomal circFNDC3B on ESCC cell growth, invasion, migration, apoptosis, and glycolysis. The regulatory network of circFNDC3B/miR-490-5p/TXNRD1 was also investigated in ESCC cells.

Materials and methods

Specimen collection

ESCC tissue samples (n = 50) and matched nearby normal tissue samples (n = 50) were harvested

from ESCC patients who received resection in Zigong Fourth People's Hospital. After being collected, tissue specimens were promptly snap-frozen in liquid nitrogen. All patients signed their written informed consents. The procedure was approved by the Research Ethics Committee of Zigong Fourth People's Hospital. Patient inclusion criteria were as follows: age 18–68 years; stage I–III ESCC; no history of other treatments; and regular follow-up after receiving treatment. Patients with diabetes, pregnancy, or previous malignancy were excluded. Follow-up was followed for 5 years after treatment, with follow-up every 3 months for the first 2 years and every 6 months for the next three years. Clinicopathologic features of ESCC patients are provided in Table 1.

Cell culture and transfection

Human normal esophageal cells (HET-1A) were provided by BeNa Culture Collection (Beijing, China) and ESCC cells (KYSE30, KYSE180, KYSE450, and EC109) were commercially provided by COBIOER (Nanjing, China) and grown in DMEM RPMI-1640 medium (Solarbio, Beijing, China) that contained 10% fetal bovine serum (FBS; Solarbio) under standard conditions (37°C, 5% CO₂).

Short hairpin RNA targeting circFNDC3B (sh-circFNDC3B#1, sh-circFNDC3B#2, and sh-circFNDC3B#3), circFNDC3B overexpression vector (circFNDC3B), miR-490-5p mimics and inhibitor (in-miR-490-5p and miR-490-5p), TXNRD1-overexpressing plasmid (TXNRD1), and their negative controls (sh-NC, Vector, in-miR-NC, miR-NC, and pcDNA) were constructed by RiboBio (Guangzhou, China). When the cell confluence reached 70%, these plasmids or/and oligonucleotides were introduced into cells using Lipofectamine 3000 Reagent (Invitrogen, Carlsbad, CA, USA).

Quantitative real-time PCR (RT-qPCR)

TRIzol reagent (Invitrogen) was utilized for isolating total RNA. The cDNA was synthesized by a Primescript RT Reagent (TaKaRa, Kusatsu, Japan) or miScript II RT kit (Invitrogen).

Table 1. Relationship between circFNDC3B expression and clinicopathologic features of esophageal squamous cell carcinoma (ESCC) patients.

| Clinical characteristics | Total (n = 50) | circFNDC3B expression | | P value |
|----------------------------|----------------|-----------------------|-----|---------|
| | | High | Low | |
| Age | | | | 0.778 |
| ≤ 60 years | 26 | 14 | 12 | |
| >60 years | 24 | 11 | 13 | |
| Gender | | | | 0.776 |
| Male | 28 | 13 | 15 | |
| Female | 22 | 12 | 10 | |
| Tumor size | | | | 0.387 |
| <5 cm | 30 | 17 | 13 | |
| ≥5 cm | 20 | 8 | 12 | |
| TNM stage | | | | 0.047* |
| I–II | 24 | 8 | 16 | |
| III | 26 | 17 | 9 | |
| Histologic differentiation | | | | 0.926 |
| Well | 23 | 11 | 12 | |
| Moderate | 18 | 9 | 9 | |
| Poor | 9 | 5 | 4 | |
| Lymph node invasion | | | | 0.047* |
| Present | 27 | 17 | 10 | |
| Absent | 23 | 8 | 15 | |

Thereafter, qPCR was run on a CFX96 system (Bio-Rad, Hercules, CA, USA) using SYBR Premix Ex Taq II (Takara) with the following reaction conditions: 40 cycles of denaturation at 95°C for 10 seconds, annealing at 60°C for 60 seconds, and elongation at 72°C for 60 seconds. The RNA levels were analyzed via 2^{-ΔΔCt} method [24]. β-actin and U6 were utilized as the reference controls for circFNDC3B/FNDC3B/TXNRD1 and miR-490-5p, respectively. Primer information is listed in Table 2.

Subcellular localization

The PARIS™ Kit (Invitrogen) was used for isolating the fractions of cytoplasm and nucleus based on the manufacturer's instructions. The expression levels of circFNDC3B, β-actin (cytoplasm control) and U6 (nucleus control) were assessed via RT-qPCR.

RNase R treatment

RNA extracted from ESCC cells was incubated added with RNase R (Seebio, Shanghai, China) and incubated for half an hour at 37°C [21]. Thereafter, circFNDC3B and FNDC3B expression levels were detected by RT-qPCR.

Table 2. Primer sequences for qPCR.

| Genes | Forward primer sequence | Reverse primer sequence |
|----------------|-------------------------------|------------------------------|
| circFNDC3B | 5'-AGTGCATTCAAGGACCTGCT-3' | 5'-GGATTTGGTCGGTCATCATC-3' |
| FNDC3B | 5'-GAAAGTCTCCCTGTTCCGACAC-3' | 5'-ACTCTGAGACCTCACAGCCACT-3' |
| miR-490-5p | 5'-GCCGAGCCATGGATCTCCAG-3' | 5'-CAGTGCCTGTCGTGGAGT-3' |
| TXNRD1 | 5'-GTTACTTGGGCATCCCTGGTGA-3' | 5'-CGCACTCCAAAGCGACATAGGA-3' |
| β -actin | 5'-GCCGGGACCTGACTGACTAC-3' | 5'-TCTCCTTAATGTCACGCACGAT-3' |
| U6 | 5'-CTCGCTTCGGCAGCACATATACT-3' | 5'-ACGCTTCACGAATTTGCGTGTC-3' |

Cell proliferation assays

For colony formation assay [25], we seeded cells into 6-well plates. After culturing for 14 days, the medium was gently removed and washed twice with PBS (Beyotime, Jiangsu, China). After fixing in 4% paraformaldehyde (Beyotime), the cells were stained using 0.1% crystal violet (Beyotime).

5-ethynyl-2'-deoxyuridine (EDU) assay [26] was conducted using the EDU kit RiboBio) to test DNA synthesis. Briefly, we seeded cells into a 24-well plate. After treatment, EdU solution (50 μ M) was put into per well for 2 h. After fixing with paraformaldehyde (4%), we treated with 0.5% Triton-X-100. Following staining with Apollo reaction for half an hour, these cells were stained using DAPI and photographed using a fluorescence microscope ($\times 200$, Leica, Wetzlar, Germany).

Migration and invasion assays

Cell migratory ability was examined through wound healing assays [27]. In short, we seeded cells into a 24-well plate. The monolayer cells were gently scratched in the middle of each well using a sterile pipette tip (200 μ L) when the cell confluence reached 80%. After incubation for 24 h, these cells were photographed with a microscope (Leica) at $\times 40$ magnification.

The transwell chambers were employed to evaluate cell invasive and migratory capacities [28]. In short, cells suspended in serum-free medium (200 μ L) were plated in the apical chamber of transwell pre-coated with (for detecting cell invasive ability) or without (for detecting cell migratory ability) Matrigel (BD Biosciences, San Jose, CA, USA). In the bottom compartment, a complete medium (600 μ L) was used as a chemoattractant. 24 h later, cells still in the top chamber were carefully removed, and invasive and

migratory cells were fixed in methanol. After staining with crystal violet solution, the cells were photographed with an inverted microscope (Leica).

Flow cytometry analysis

Annexin V-FITC/PI apoptosis detection kit purchased from Sangon (Shanghai, China) was utilized for detection of apoptosis in accordance with the manufacturer's instructions. In short, cells were digested and harvested. After resuspending in binding buffer (0.4 mL), the cells were dyed with Annexin V-FITC and PI for half an hour, followed by measuring apoptotic cells using flow cytometer (BD Biosciences).

Western blot (WB) assay

Protein extraction reagent (Beyotime) and BCA protein quantification reagent (Abcam, Cambridge, UK) were used for protein extraction and quantification respectively. WB was executed according to a previous report [29]. The extracted protein samples were separated using SDS-PAGE (Beyotime), followed by transferring to nitrocellulose membranes (Invitrogen). After blockage with nonfat milk (5%; Beyotime), the antibodies listed below were applied to incubate these membranes for 12–14 h at 4°C: Bcl-2 (ab194583, 1:1500, Abcam), Bax (ab32503, 1:1500, Abcam), glucose transport protein type 1 (GLUT1; ab150299, 1:3000, Abcam), LDHA (ab125683, 1:2000, Abcam), TXNRD1 (ab124954, 1:1500, Abcam) or β -actin (ab227387, 1:3000, Abcam). After incubation of the corresponding secondary antibody (ab205718, 1:6000, Abcam), protein blot visualization was achieved by an ECL reagent (Abcam). Analysis of relative levels of proteins was performed by densitometric analysis using Image J software (Bio-Rad).

Glycolysis detection

Lactate Assay Kit and Glucose Assay Kit (BioVision, Milpitas, CA, USA) were applied for examining lactate production and glucose consumption, following the manufacturer's protocols. Glucose consumption was the amount of glucose in the control medium without cells minus the amount of glucose in the medium inoculated with cells. Glucose consumption and lactate production results were normalized to total cellular protein.

In vivo tumor growth assay

BALB/c male nude mice (n = 24; weighing 18–25 g; 5–6 weeks old) were commercially provided by Vital River (Beijing, China). We randomly divided these mice into 4 groups with 6 mice in each group: sh-NC, sh-circFNDC3B, Exo-sh-NC, and Exo-sh-circFNDC3B. EC109 cells suspended in PBS ($5 \times 10^6/0.2$ mL) were injected into the right flank of nude mice. We measured tumor volume using calipers every 7 days and calculated using the following formula: $\frac{1}{2} \times \text{width}^2 \times \text{length}$. After 28 days, these mice were sacrificed. All mice were reared in specific pathogen-free conditions and killed by cervical dislocation euthanasia. Tumor tissue excised from dead mice was used for further analysis. All animal experiments are approved by the Animal Care and Use Committee of Zigong Fourth People's Hospital.

Exosome isolation and identification

Isolation of exosomes was conducted using the ExoQuick precipitation kit (System Biosciences, Mountain view, CA, USA) according to the manufacturer's instructions. Briefly, 500 μL of ExoQuick Exosome Precipitation Solution was mixed with 250 μL of cell supernatant sample and incubated at 4°C. After 30 minutes, centrifugation (30 minutes, $1500 \times g$) was performed and the supernatant was discarded. Second centrifugation of the sample (5 minutes, $1500 \times g$) was done to obtain the pellet. The pellets were resuspended in 100 μL PBS and stored at -80°C .

Transmission electron microscopy (TEM)

Phosphate-buffered saline-washed exosomes fixed with 4% paraformaldehyde were placed on a formvar 200 mesh copper grid for 20 minutes at room temperature. After fixation in 1% glutaraldehyde for 5 minutes, samples were stained with uranyl oxalate for 5 minutes, followed by the addition of 4% uranyl acetate and 2% methylcellulose at a ratio of 1:9 on ice. Finally, TEM (Hitachi, Ltd., Tokyo, Japan) was used for imaging [30].

Nanoparticle tracking analysis (NTA)

Exosomes were resuspended in PBS (5 $\mu\text{g}/\text{mL}$). The sample was manually injected into the sample chamber at ambient temperature. Each sample was measured in triplicate with a camera setting of 13 with an acquisition time of 30 seconds and a detection threshold setting of 7. Finally, data were analyzed using NTA analysis software (NanoSight technology, Malvern, UK) [31].

Establishment of cell co-culture model

To probe the role of the exosomal circFNDC3B in the recipient cells, a co-culture model was built according to a previous research [32]. Cells were assigned to Exo-sh-NC group (donor KYSE450 and EC109 cells transfected with sh-NC were co-cultured with KYSE450 and EC109 cells), Exo-sh-circFNDC3B#1 group (donor KYSE450 and EC109 cells transfected with sh-circFNDC3B#1 were co-cultured with KYSE450 and EC109 cells), Exo-sh-circFNDC3B#1 + in-miR-NC (donor KYSE450 and EC109 cells co-transfected with sh-circFNDC3B#1 + in-miR-NC were co-cultured with KYSE450 and EC109 cells) Exo-sh-circFNDC3B#1 + in-miR-490-5p (donor KYSE450 and EC109 cells co-transfected with sh-circFNDC3B#1 + in-miR-490-5p were co-cultured with KYSE450 and EC109 cells). After 48 h of transfection, donor cells (KYSE450 and EC109 cells, 1×10^5 cells per well) were collected and inoculated into the top chamber of transwell culture plate. Recipient cells (KYSE450 and EC109 cells) were inoculated into the bottom chamber of Transwell 1 day in advance. After co-culturing

apical and basolateral chambers, the recipient cells were collected for further research.

Dual-luciferase reporter assay

The association between miR-490-5p and circFNDC3B or TXNRD1 was predicted using circinteractome or TargetScan. CircFNDC3B or TXNRD1 fragments including the miR-490-5p binding site region and the corresponding mutated region were synthesized and individually cloned into the pmirGLO vectors (Promega, Madison, WI, USA) to create wild-type reporter and mutated-type vectors (circFNDC3B WT/MUT and TXNRD1 3'UTR WT/MUT). Then, the constructed reporter plasmid was introduced into KYSE450 and EC109 cells together with miR-NC/miR-490-5p for 48 h. Detection of the luciferase activity was performed using dual-luciferase reporter assay system (Promega). Data for firefly luciferase activity were normalized to Renilla luciferase activity.

RNA pull-down assay

Biotinylated negative control (Bio-NC) and biotinylated circFNDC3B WT/MUT (Bio-circFNDC3B WT/MUT) were obtained from (RiboBio) and incubated with KYSE450 and EC109 cell lysates [33]. The streptavidin magnetic beads (Invitrogen) were added to the above complex, followed by incubation for 0.5 h. Next, the mixture was washed, and the RNA complexes were extracted. At last, the enrichment of miR-490-5p was tested by RT-qPCR.

RNA immunoprecipitation (RIP) assay

RIP assay was conducted with EZ-Magna RIP Kit (Millipore, Billerica, MA, USA) following the steps provided by the manufacturer. After lysing by RIPA buffer (P0013D, Beyotime), cell lysate was treated with magnetic beads conjugated with an antibody against immunoglobulin G (Anti-IgG; as a control) or Argonaute2 (Anti-AGO2). After incubation with Proteinase K, the levels of relevant RNAs were tested via RT-qPCR.

Immunohistochemistry (IHC)

Tumor tissues were fixed in formaldehyde (10%), embedded in paraffin, followed by cutting at a thickness of 4 μ m slides. Next, these sections were incubated with the TXNRD1 (ab124954, 1:200, Abcam) antibody overnight at 4°C to measure TXNRD1 expression. After incubation with secondary antibody (ab150077, 1:1000, Abcam). After staining with diaminobenzidine (DAB; Beyotime) and counterstaining with hematoxylin (Beyotime), the images were obtained under a microscope (Leica). The TXNRD1 score was defined as the percentage of TXNRD1-positive staining cells in the total number of cancer cells.

Statistical analysis

Data from at least 3 independent experiments were displayed as mean \pm standard deviation and analyzed by GraphPad Prism 7.0. Differences between the different groups were analyzed via Student's *t*-test and analysis of variance. For evaluating the diagnostic value of circFNDC3B for ESCC, the receiver operating characteristics (ROC) curve was constructed. Overall survival was defined as the time interval from surgery to death. The Kaplan-Meier method was used to calculate OS, with the log-rank method to determine the significance of differences. A significant difference was represented when $P < 0.05$.

Results

In this paper, we examined the effect of circFNDC3B and exosomal circFNDC3B on ESCC cell malignancy and glycolysis. The regulatory network of circFNDC3B/miR-490-5p/TXNRD1 was also investigated in ESCC cells.

CircFNDC3B was overexpressed in ESCC tissues and cells

To identify the circRNAs involved in ESCC tumorigenesis, we first searched the GEO database (accession number GSE131969). We selected the top 10 circRNAs with the most up- and down-regulation in the database to draw a heat map (Figure 1). And 5 circRNAs

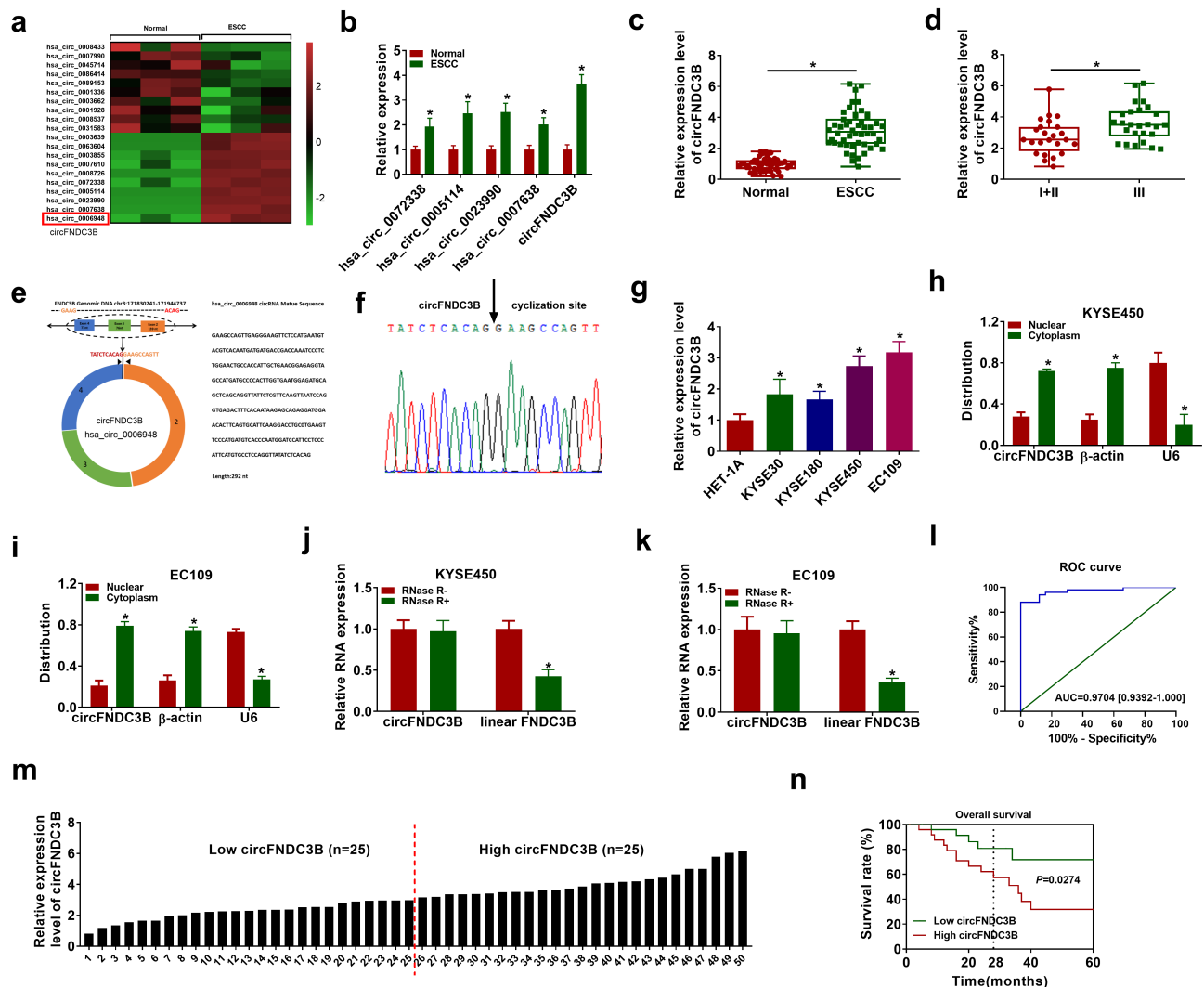


Figure 1. CircFNDC3B was overexpressed in ESCC. (a) The heat map of GSE131969 showed the expression of 20 circRNAs in normal and ESCC tissues. (b) Hsa_circ_0072338, hsa_circ_0005114, hsa_circ_0023990, hsa_circ_0007638, and circFNDC3B expression levels in normal and ESCC tissues were detected by RT-qPCR (two-way ANOVA). (c) CircFNDC3B expression in ESCC tissues ($n = 39$) and normal tissues ($n = 39$) was determined (Student's t -test). (d) The expression of circFNDC3B was determined in patients with clinical stages I + II and III (Student's t -test). (e, f) The information of circFNDC3B was presented, and Sanger sequencing confirmed the head-to-tail splicing junction of circFNDC3B. (g) The expression of circFNDC3B in ESCC cells (KYSE30, KYSE180, KYSE450, and EC109) and HET-1A cells was measured via RT-qPCR (one-way ANOVA). (h, i) The subcellular location of circFNDC3B in KYSE450 and EC109 cells was determined by RT-qPCR (two-way ANOVA). (j, k) CircFNDC3B and linear FNDC3B expression levels were determined after treatment of RNase R by RT-qPCR in KYSE450 and EC109 cells (two-way ANOVA). (l) The diagnostic effect was evaluated by ROC curve in ESCC patients (Clopper-Pearson). (m) ESCC patients were divided into low ($n = 19$) and high ($n = 20$) circFNDC3B expression groups according to the median value of circFNDC3B expression. (n) The survival rate was analyzed between low and high circFNDC3B expression groups in ESCC patients (Log-rank (Mantel-Cox) test). * $P < 0.05$.

(hsa_circ_0072338, hsa_circ_0005114, hsa_circ_0023990, hsa_circ_0007638, hsa_circ_0006948) were verified to be upregulated in ESCC, of which hsa_circ_0006948 (circFNDC3B) was upregulated the most (Figure 1(b)). Therefore, circFNDC3B was selected for further research. Further experiments verified the elevation of circFNDC3B in

ESCC tissue samples (Figure 1(c)). High expression level of circFNDC3B was significantly associated with TNM stage and lymph node invasion, but not with age, gender, tumor size, and histologic differentiation (Table 1). In addition, circFNDC3B expression was higher in tumors from patients with clinical stage III than tissues from patients with clinical stages

I + II (Figure 1(d)). CircFNDC3B, located on chr3:171830241–171944737, is generated from exons 2–4 of the FNDC3B, and its spliced length is 292 nt (Figure 1(e)). Sanger sequencing confirmed the head-to-tail splicing of circFNDC3B (Figure 1(f)). In contrast to HET-1A cells, circFNDC3B was upregulated in ESCC cells (KYSE30, KYSE180, KYSE450, and EC109), especially in KYSE450 and EC109 cells (Figure 1(g)). Therefore, KYSE450 and EC109 cells were chosen for further research. Moreover, circFNDC3B was observed to be predominantly located in the cytoplasm Figure 1(h, i). Furthermore, RNase R digestion assay showed that the circular isoform (circFNDC3B) was resistant to RNase R with respect to linear FNDC3B Figure 1(j,k). Actinomycin D treatment decreased the half-life of FNDC3B mRNA (about 10 hours), but the half-life of circFNDC3B exceeded 24 hours (Supplementary Figure S2(a,b)). These results highlighted the stability of circFNDC3B. The ROC curves revealed that circFNDC3B was able to discriminate the ESCC tissues from the normal tissues with relatively satisfactory accuracy, and the AUC value was 0.9043 (Figure 1(l)). According to the median value of circFNDC3B expression, ESCC patients were divided into low (n = 19) and high (n = 20) circFNDC3B expression groups (Figure 1(m)), and patients with high circFNDC3B expression had poor survival (dotted line represents median survival time) (Figure 1(n)).

CircFNDC3B knockdown inhibited the malignant behaviors of ESCC cells

We silenced circFNDC3B expression in KYSE450 and EC109 cells to probe the biological function of circFNDC3B in ESCC. CircFNDC3B expression was reduced in KYSE450 and EC109 cells after transfection with sh-circFNDC3B#1, sh-circFNDC3B#2 or sh-circFNDC3B#3, and circFNDC3B expression was the lowest in sh-circFNDC3B#1 group (Figure 2(a)). Hence, sh-circFNDC3B#1 was chosen for further research. The colony-forming ability of circFNDC3B-downregulating cells was reduced compared to control cells (Figure 2(b)). EdU assay showed

that circFNDC3B knockdown restrained DNA synthesis (Figure 2(c)). CircFNDC3B silencing inhibited KYSE450 and EC109 cell migration and invasion (Figure 2(d–f)) and broken line diagrams on changes in cell wound closure area were presented in Supplementary Figure S1(a,b).

CircFNDC3B knockdown induced cell apoptosis, lessened cell glycolysis, reduced xenograft tumor growth

Flow cytometry analysis indicated that interference of circFNDC3B induced KYSE450 and EC109 cell apoptosis (Figure 3(a)). As expected, circFNDC3B knockdown reduced Bcl-2 protein abundance and increased Bax protein abundance Figure 3(b,c). Most fast-growing malignant cells get more energy through glycolysis [34]. GLUT1 and LDHA protein levels were reduced after downregulation of circFNDC3B Figure 3(d,e). Consistently, circFNDC3B knockdown was able to inhibit glycolysis through suppressing glucose consumption and lactate production Figure 3(f,g). To evaluate the role of circFNDC3B in ESCC *in vivo*, sh-NC or sh-circFNDC3B#1-transfected EC109 cells were injected into nude mice. Deficiency of circFNDC3B could decrease tumor growth by reducing tumor volume and weight Figure 3(h,i).

CircFNDC3B was transmitted by exosomes in ESCC cells

Exosomes secreted by cancer cells contain a large amount of RNAs, including circRNAs lncRNAs and miRNAs [9]. Therefore, we explored whether circFNDC3B was able to transmit via exosomes in ESCC cells. Exosomes were isolated from KYSE450 and EC109 cell medium and the morphology of exosomes was observed using TEM (Figure 4(a)). The exosomal markers (CD81 and CD63) were identified using WB analysis, indicating that exosomes were successfully enriched (Figure 4(b)). The size of the exosomes was exhibited in Figure 4(c). Next, we established a cell co-culture model. The expression of circFNDC3B in donor cells (KYSE450 and EC109), exosomes, and recipient cells (KYSE450 and EC109) was determined by RT-qPCR after introduction with circFNDC3B and sh-circFNDC3B. CircFNDC3B

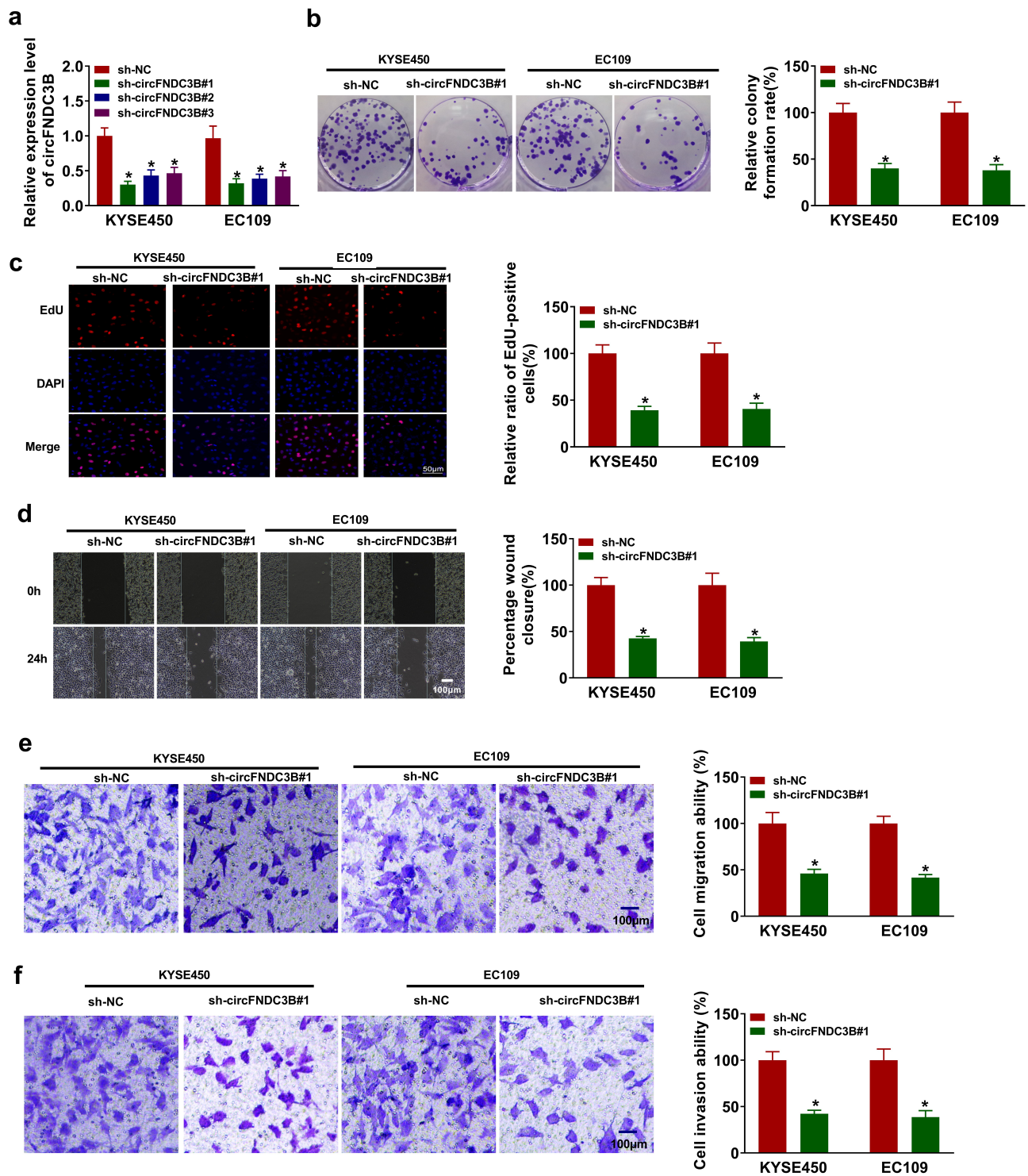


Figure 2. Interference of circFND3B suppressed ESCC progression. (a) CircFND3B expression was determined in KYSE450 and EC109 cells transfected with sh-NC, sh-circFND3B#1, sh-circFND3B#2, or sh-circFND3B#3 (two-way ANOVA). (b-g) KYSE450 and EC109 cells were transfected with sh-NC or sh-circFND3B#1. (b) Colony formation assay assessed colony formation ability (two-way ANOVA). (c) EdU assay detected DNA synthesis ($\times 200$) (two-way ANOVA). (d) Wound healing assay detected cell migratory ability ($\times 40$) (two-way ANOVA). (e,f) Transwell assay determined cell migration and invasion ($\times 100$) (two-way ANOVA). * $P < 0.05$.

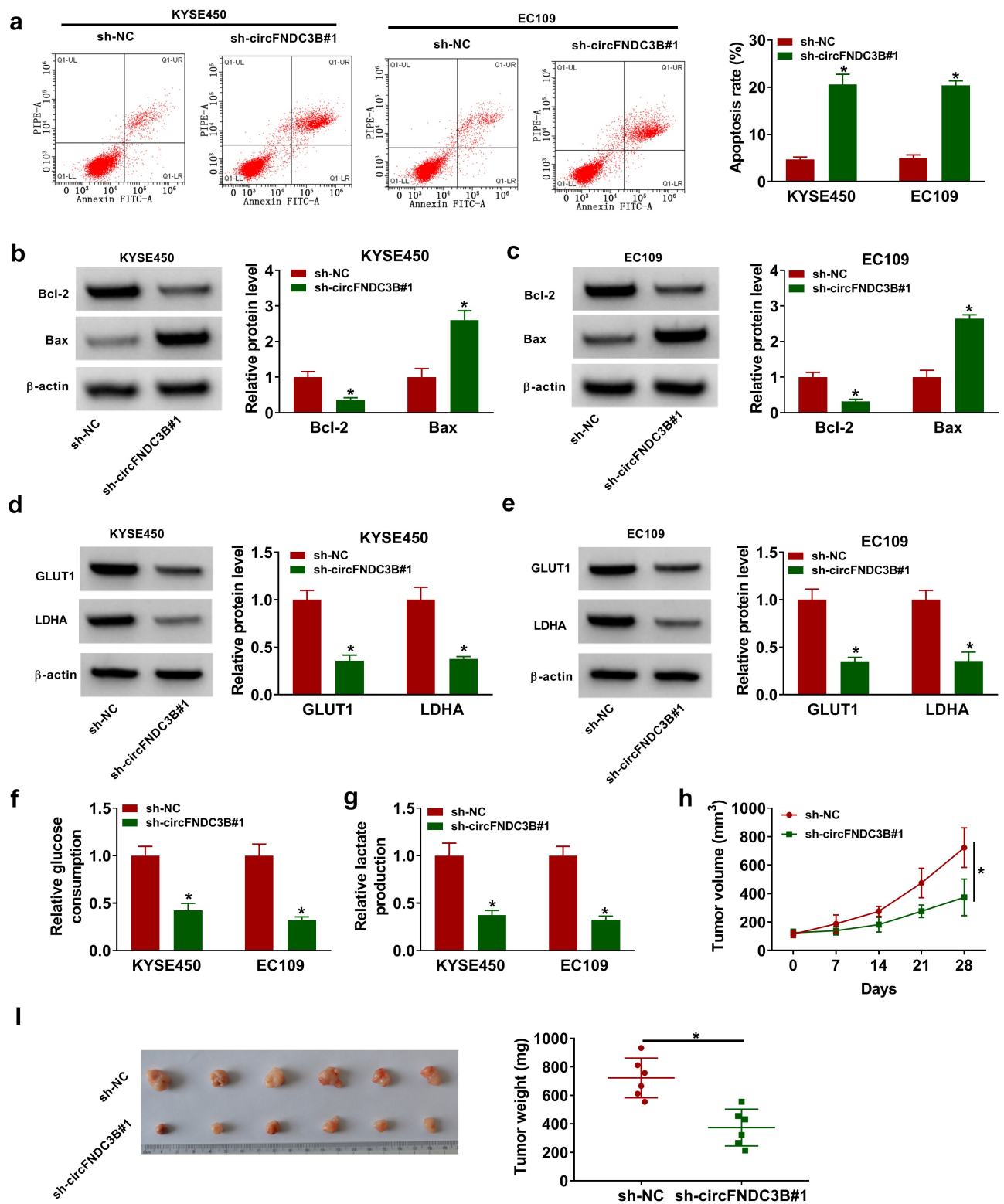


Figure 3. Interference of circFND3B decreased cell glycolysis in ESCC cells. (a) Detection of cell apoptosis was conducted in ESCC cells transfected with sh-NC or sh-circFND3B#1 via flow cytometry analysis (two-way ANOVA). (b,c) WB assay was used for testing Bcl-2 and Bax protein levels in the above cells (two-way ANOVA). (d,e) GLUT1 and LDHA protein levels were analyzed by WB in the above cells (two-way ANOVA). (f,g) Glucose consumption and lactate production were detected using corresponding kits in the above cells (two-way ANOVA). (h,i) EC109 cells stably introduced with sh-NC or sh sh-circFND3B#1 were introduced into nude mice. Tumor volume was recorded and tumor weight was detected (Student's *t*-test). **P* < 0.05.

expression was observed to be elevated in donor cells (KYSE450 and EC109), exosomes and recipient cells (KYSE450 and EC109) after introduction with circFNDC3B, and declined in donor cells, exosomes and recipient cells following transfection with sh-circFNDC3B#1 (Figure 4(d–i)). These data indicated that circFNDC3B could be delivered through exosomes in ESCC cells.

Reduction of exosomal circFNDC3B inhibited ESCC cell progression

Co-cultivation model was established to determine the action of exosomal circFNDC3B. After co-culturing the donor cells (with sh-circFNDC3B#1) and recipient cells for 48 h, the effects of exosomal circFNDC3B were detected. We discovered that there was a decrease in cell colony formation, proliferation, migration, and invasion in the Exo-sh-circFNDC3B#1 group, while an elevation in cell apoptosis (Figure 5(a–f)) and color images of wound closure, cell apoptosis, and cell invasion experiments were presented in Supplementary Figure S6(a–c). Bcl-2 protein level was reduced but Bax protein level was increased in the Exo-sh-circFNDC3B#1 group (Figure 5(g,h)). In addition, co-culturing with sh-circFNDC3B#1-transfected donor cells decreased glucose consumption, lactate production, and protein expression of GLUT1 and LDHA in recipient cells (Figure 5(i–l)). Our results showed that donor cells-derived exosome-shuttling circFNDC3B could affect the behaviors of recipient cells.

CircFNDC3B was a sponge of miR-490-5p

We then predicted the potential target miRNAs of circFNDC3B using circinteractome. miR-490-5p had binding sites with circFNDC3B, as exhibited in Figure 6(a). Overexpression and inhibition efficiency of miR-490-5p were examined using RT-qPCR (Figure 6(b)). Co-transfection of circFNDC3B WT and miR-490-5p resulted in a reduction in the luciferase activity in KYSE450 and EC109 cells, and co-transfection of circFNDC3B WT and in-miR-490-5p increased the luciferase activity (Figure 6(c,d)). The enrichment of circFNDC3B and miR-490-5p was found to be high in Anti-AGO2 group with respect to

Anti-IgG group (Figure 6(e,f)). Meanwhile, Bio-circFNDC3B WT led to higher miR-490-5p enrichment (Figure 6(g,h)). And miR-490-5p level was reduced in ESCC tissue samples and cell lines (Figure 6(i,j)). In addition, circFNDC3B deficiency increased miR-490-5p abundance in KYSE450 and EC109 cells, but the elevated abundance of miR-490-5p was reversed after in-miR-490-5p introduction (Figure 6(k)).

Exosomal circFNDC3B modulated the behaviors of ESCC cells through sponging miR-490-5p

Next, we further explored whether exosomal circFNDC3B regulated ESCC progression by sponging miR-490-5p. MiR-490-5p expression was found to be increased in Exo-sh-circFNDC3B#1 group, while its elevation was weakened after in-miR-490-5p introduction (Figure 7(a)). Moreover, introduction of in-miR-490-5p reversed the effects of Exo-sh-circFNDC3B#1 on cell growth, migration, invasion, and apoptosis (Figure 7(b–g)) and color images of wound closure, cell apoptosis, and cell invasion experiments were presented in Supplementary Figure S7(a–c). The changes in Bcl-2 and Bax protein levels in recipient cells with Exo-sh-circFNDC3B#1 treatment were overturned by miR-490-5p inhibition (Figure 7(h–i)). Moreover, the decrease of glucose consumption, lactate production, and protein levels of GLUT1 and LDHA caused by Exo-sh-circFNDC3B#1 was reversed by miR-490-5p silencing (Figure 7(j–m)). To sum up, exosomal circFNDC3B exerted its function in ESCC cells through interacting with miR-490-5p.

TXNRD1 was targeted by miR-490-5p

To identify the target of miR-490-5p, we used a bioinformatics tool (TargetScan). Among the predicted targets, 7 (SOX6, PPM1L, FZD3, CDC25A, TXNRD1, LASP1, E2F3) genes that have been studied in ESCC were selected for analysis. RT-qPCR results showed that overexpression of miR-490-5p inhibited the mRNA levels of FZD3, CDC25A, TXNRD1 and E2F3, and TXNRD1 with the most differential change was selected for further exploration. As presented in Figure 8(a), TXNRD1 3'UTR possessed the

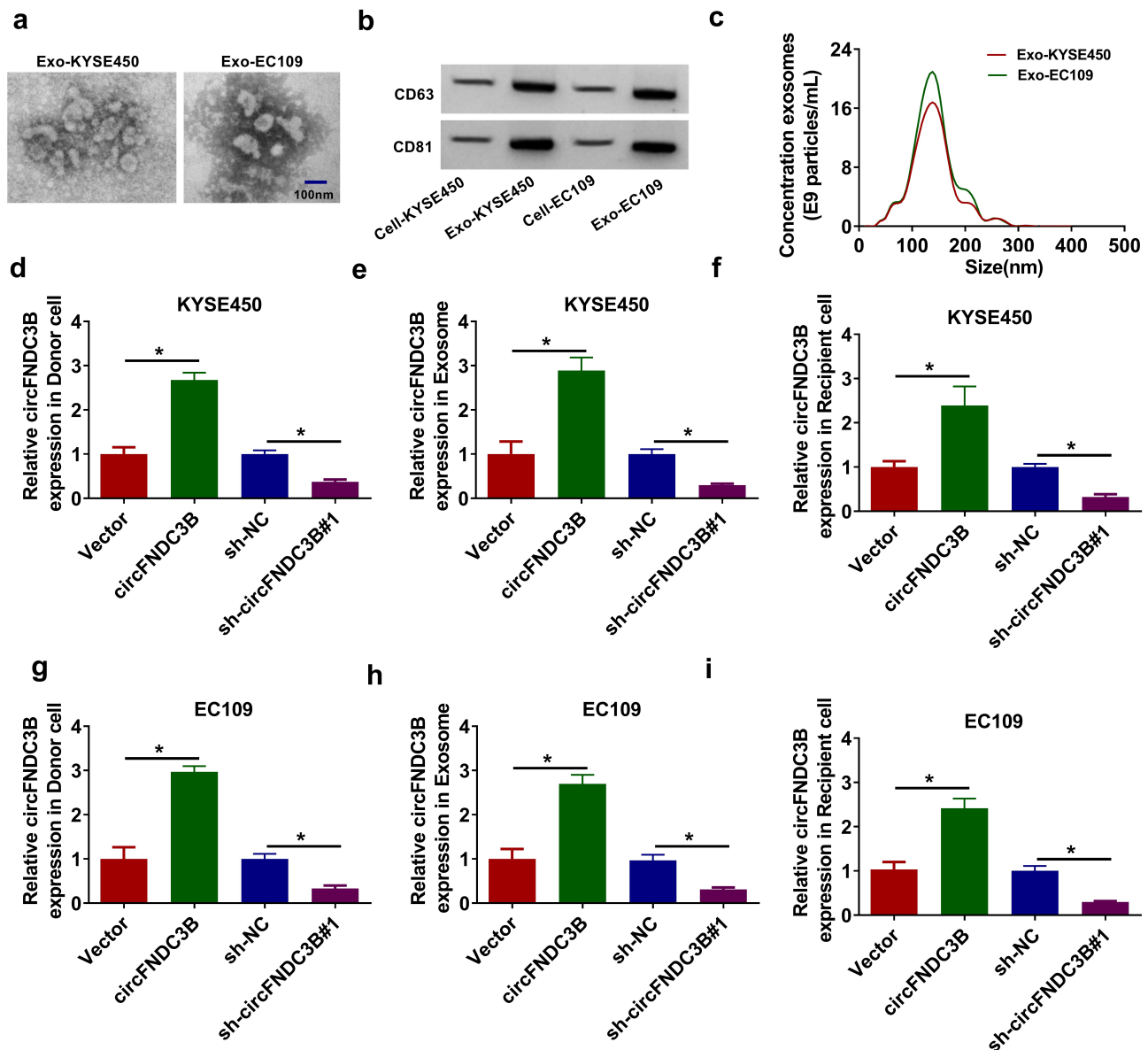


Figure 4. CircFNDC3B was delivered through exosomes in ESCC cells. (a) Exosomes were isolated from KYSE450 and EC109 cell medium and the morphology of isolated exosomes was observed by TEM. (b) WB assay was used for detecting exosomal markers (CD63 and CD81) protein levels in exosomes (Exo-KYSE450/EC109) and cell extracts (Cell-KYSE450/EC109). (c) The size of exosomes was analyzed NTA. (d-i) CircFNDC3B expression in donor KYSE450 and EC109 cells (transfected with Vector, circFNDC3B, sh-NC, or sh-circFNDC3B#1), exosomes, and recipient KYSE450 and EC109 cells was determined using RT-qPCR (one-way ANOVA). * $P < 0.05$.

possible binding sequence for miR-490-5p. We also observed that miR-490-5p overexpression decreased TXNRD1 3'UTR WT luciferase activity and miR-490-5p downregulation increased TXNRD1 3'UTR WT luciferase activity [Figure 8 \(b,c\)](#). In ESCC tissues, TXNRD1 mRNA and protein levels were increased in contrast to normal tissues [Figure 8\(d,e\)](#). Likewise, TXNRD1 protein levels were also enhanced in ESCC cells in contrast to HET-1A cells ([Figure 8\(f\)](#)). Also, Pearson

correlation coefficient analysis showed that the expression of miR-490-5p in ESCC samples was negatively correlated with circFNDC3B and TXNRD1 mRNA, while the expression levels of circFNDC3B and TXNRD1 mRNA were positively correlated ([Figure 8\(g-i\)](#)). In addition, we found that TXNRD1 protein levels were reduced after miR-490-5p transfection, which was rescued by co-transfection of TXNRD1 ([Figure 8\(j\)](#)). The data showed that circFNDC3B silencing inhibited

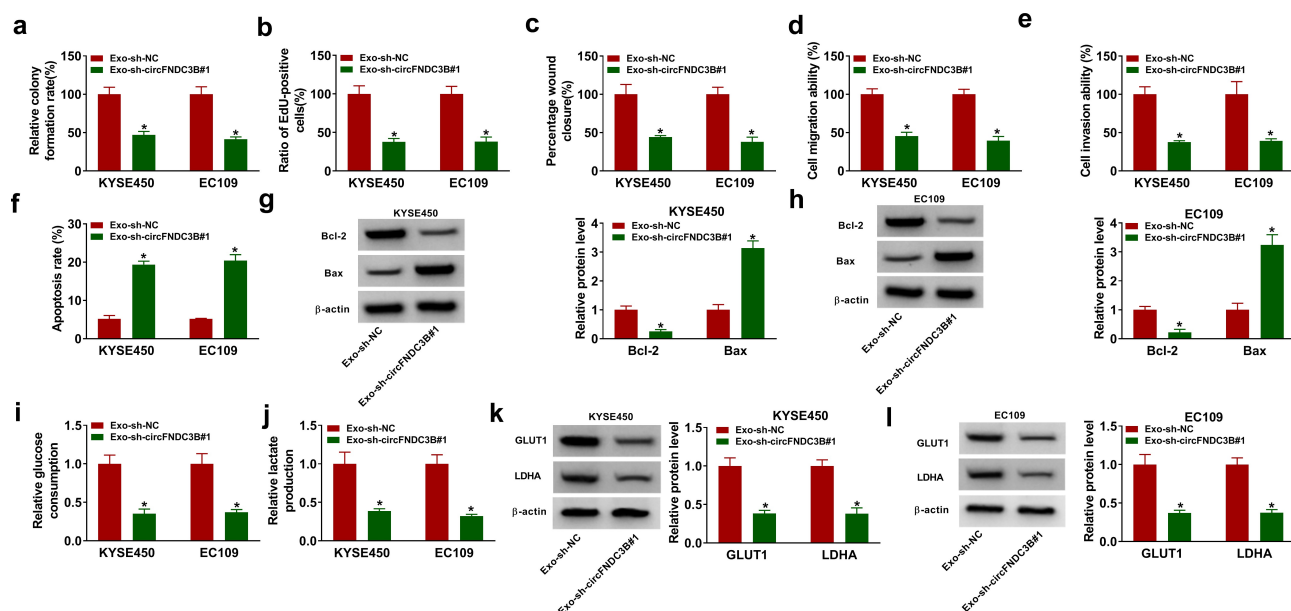


Figure 5. Decreasing exosomal circFNDC3B inhibited ESCC cell progression. Donor KYSE450 and EC109 cells transfected with sh-NC or sh-circFNDC3B#1 were co-cultured with recipient KYSE450 and EC109 cells. (a,b) Cell proliferation was detected (two-way ANOVA). (c-e) Cell migratory and invasive abilities were examined (two-way ANOVA). (f) Cell apoptosis was detected (two-way ANOVA). (g,h) Bcl-2 and Bax protein levels were tested (two-way ANOVA). (i,j) Glucose consumption and lactate production were examined (two-way ANOVA). (k,l) GLUT1 and LDHA protein levels were examined (two-way ANOVA). * $P < 0.05$.

TXNRD1 protein levels in KYSE450 and EC109 cells, which were impaired by inhibiting miR-490-5p (Figure 8(k)), indicating that circFNDC3B sponged miR-490-5p to positively modulate TXNRD1 expression.

Upregulation of miR-490-5p repressed ESCC cell malignant features by targeting TXNRD1

Considering that TXNRD1 was targeted by miR-490-5p in ESCC cells, we further explored whether miR-490-5p exerted its roles via targeting TXNRD1. Overexpression of miR-490-5p was able to suppress cell colony formation, proliferation, migration, and invasion, while TXNRD1 elevation abated these effects (Figure 9(a-e)) and color images of wound closure, cell apoptosis, and cell invasion experiments were presented in Supplementary Figure S8(a-c). In addition, miR-490-5p upregulation induced cell apoptosis and elevated Bax protein levels as well as decreased Bcl-2 protein levels, which could be counteracted by elevating TXNRD1 (Figure 9(f-h)). Meanwhile,

enforced expression of miR-490-5p reduced glucose consumption, lactate production, and the protein levels of GLUT1 and LDHA while these changes were weekend by elevation of TXNRD1 (Figure 9(i-l)). In addition, whether TXNRD1 is associated with circFNDC3B-mediated effects on ESCC cells was explored. The results showed that TXNRD1 overexpression weakened the effects of circ_FNDC3B knockdown on ESCC cell proliferative, migrating, and invading, and apoptotic capacities (Supplementary Figures S4(a-g)). Also, the effects of circ_FNDC3B inhibition on Bcl-2 and Bax protein levels were lowered after TXNRD1 introduction (Supplementary Figures S5(a,b)). As expected, the decreased levels of glucose consumption and lactate production, as well as GLUT1 and LDHA proteins

Decreasing exosomal circFNDC3B inhibited tumor growth *in vivo*

We established mice xenograft models to determine the function of exosomal circFNDC3B

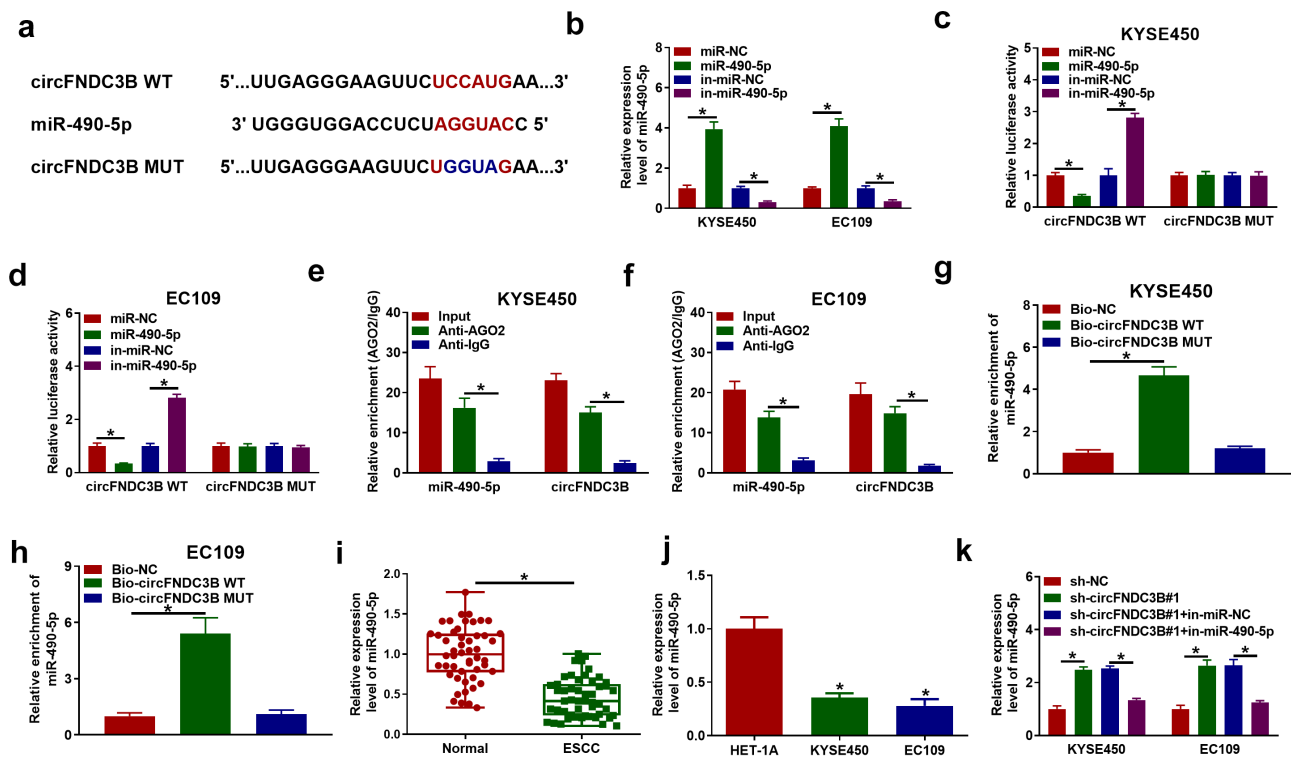


Figure 6. MiR-490-5p directly targeted circFNDC3B. (a) The potential binding sites between circFNDC3B and miR-490-5p were predicted by circinteractome. (b) MiR-490-5p level was detected in KYSE450 and EC109 cells transfected with miR-NC, miR-490-5p, in-miR-NC, or in-miR-490-5p (two-way ANOVA). (c,d) The luciferase activity in KYSE450 and EC109 cells co-transfected with circFNDC3B WT/MUT and miR-NC/miR-490-5p or in-miR-NC/in-miR-490-5p was determined (two-way ANOVA). (e,f) CircFNDC3B and miR-490-5p enrichment were examined in KYSE450 and EC109 cells by RIP assay (two-way ANOVA). (g,h) CircFNDC3B and miR-490-5p enrichment was examined by RNA pull-down assay in KYSE450 and EC109 cells incubated with Bio-NC, Bio-circFNDC3B WT, or Bio-circFNDC3B MUT (one-way ANOVA). (i,j) MiR-490-5p expression was measured by RT-qPCR in normal tissues, ESCC tissues, HET-1A cells, and ESCC cells (KYSE450 and EC109) (Student's *t*-test and one-way ANOVA). (k) MiR-490-5p expression was examined in KYSE450 and EC109 cells transfected with sh-NC, sh-circFNDC3B#1, sh-circFNDC3B#1 + in-miR-NC, or sh-circFNDC3B#1 + in-miR-490-5p (two-way ANOVA). **P* < 0.05.

in vivo. As presented in Figures 10(a,b)), the volume and weight of tumors were inhibited in the Exo-sh-circFNDC3B#1 group relative to the Exo-sh-NC group. Also, circFNDC3B expression and TXNRD1 protein levels were declined in Exo-sh-circFNDC3B#1 group in comparison with Exo-sh-NC group, but miR-490-5p expression was increased (Figure 10(c-e)). IHC analysis showed that TXNRD1 expression in the Exo-sh-circFNDC3B#1 group was lower than that in the Exo-sh-NC group (Figure 10(F)).

Discussion

ESCC is a frequent malignancy in the digestive system [35]. Exosomes are implicated in the regulating tumor-normal communication in the

tumor microenvironment [36]. Recently, it has been demonstrated that circRNAs contained in exosomes are promising biomarkers for cancers and have critical roles in cancer development. For instance, exosomal circ-ZNF652 promoted hepatocellular carcinoma cell metastasis, proliferation, and glycolysis through modulation of the miR-29a-3p/GUCD1 axis [37]. Exosomal circSHKBP1 contributed to gastric cancer progression by modulating miR-582-3p/HUR/VEGF axis and limiting HSP90 degradation [38]. In this research, we mainly probed into the role of exosomal circFNDC3B in ESCC progression.

It was revealed that high levels of circ_0006948 were associated with advanced breast cancer, lymph node metastasis, and distant metastasis, and knock-down of circ_0006948 reduced the proliferative and

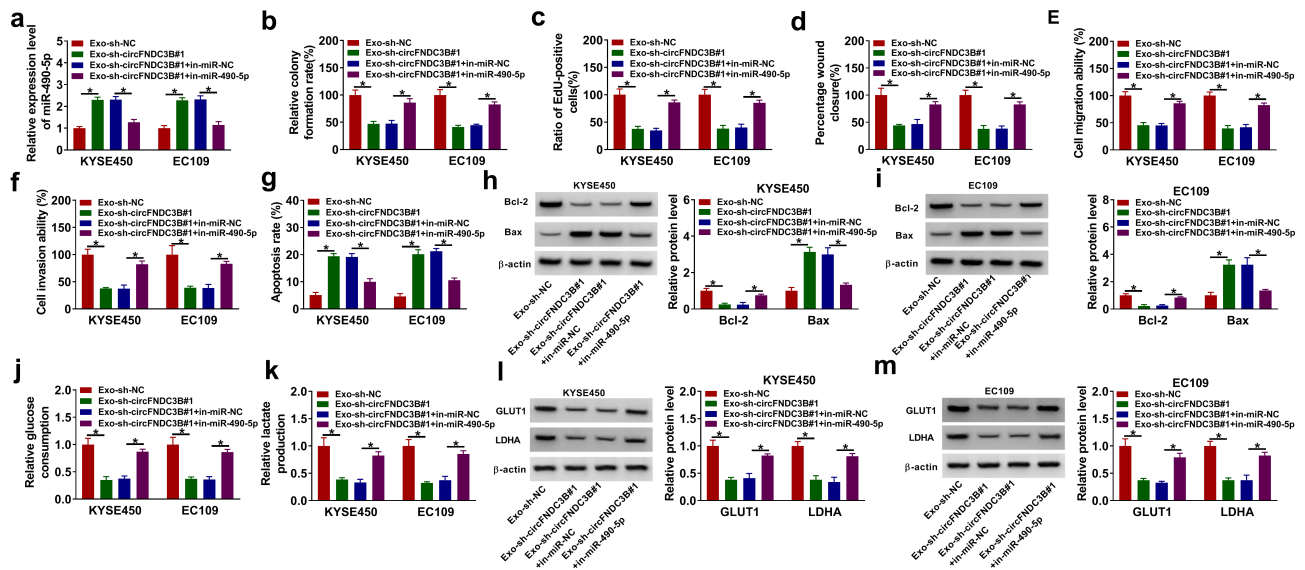


Figure 7. Exosomal circFND3B exerted its function in ESCC cells through sponging miR-490-5p. Donor KYSE450 and EC109 cells transfected with sh-NC, sh-circFND3B#1, sh-circFND3B#1 + in-miR-NC, or sh-circFND3B#1 + in-miR-490-5p were co-cultured with recipient KYSE450 and EC109 cells. (a) MiR-490-5p level was determined (two-way ANOVA). (b,c) Cell proliferative ability was detected. (d-f) Cell migratory and invasive capacities were detected (two-way ANOVA). (g) Cell apoptosis was determined (two-way ANOVA). (h and i) Bcl-2 and Bax protein levels were detected (two-way ANOVA). (j,k) Glucose consumption and lactate production were examined (two-way ANOVA). (l,m) GLUT1 and LDHA protein levels were detected (two-way ANOVA). * $P < 0.05$.

metastatic abilities of cancer cells [39]. CircFND3B has been exposed to exert a tumor-promoting role in EC. Yue *et al.* uncovered that high levels of circ_0006948 were gained in EC tissues and cells, and circFND3B promoted EC cell growth, EMT, mobility, and invasion through regulation of the miR-4262/FND3B axis [40]. Moreover, circFND3B was overexpressed in ESCC cells and tissues, and circFND3B facilitated ESCC cell proliferative, migratory and invasive abilities through the miR-490-3p/HMGA2 axis [14]. Another report displayed that circ_0006948 knockdown lowered the glycolytic, proliferative, migrating, and invading capacities of ESCC cells via mediation of the miR-3612/LASP1 axis [41]. In agreement with these researches, an increase of circFND3B expression was also detected in ESCC tissues and cells, and circ_0006948 knockdown lowered ESCC cell glycolytic, proliferative, migrating, and invading capacities. Moreover, circFND3B could distinguish ESCC tissues from normal tissues, indicating that

circFND3B was a potential diagnostic marker for ESCC, and patients with high circFND3B expression displayed a poorer survival rate. *In vivo* assay confirmed that circFND3B downregulation also repressed tumor growth *in vivo*. Nevertheless, the function of exosomal circFND3B in ESCC cells is unclear. The novelty of this study was the observation that circFND3B could be transmitted from cell to cell via exosomes. The proliferative, migratory, invasive, and glycolytic abilities of recipient ESCC cells were impaired after co-incubation with exosomal circFND3B-knockdown donor cells. Furthermore, the growth ability of recipient ESCC cells incubated with exosomal circFND3B knockdown donor cells was also reduced in mice. These data highlighted that cell-derived exosomal circFND3B promoted ESCC growth.

Mechanistically, circRNAs perform their functional roles in human malignant tumors via interacting with miRNAs to regulate target gene expression [42]. Next, we validated that miR-490-5p was

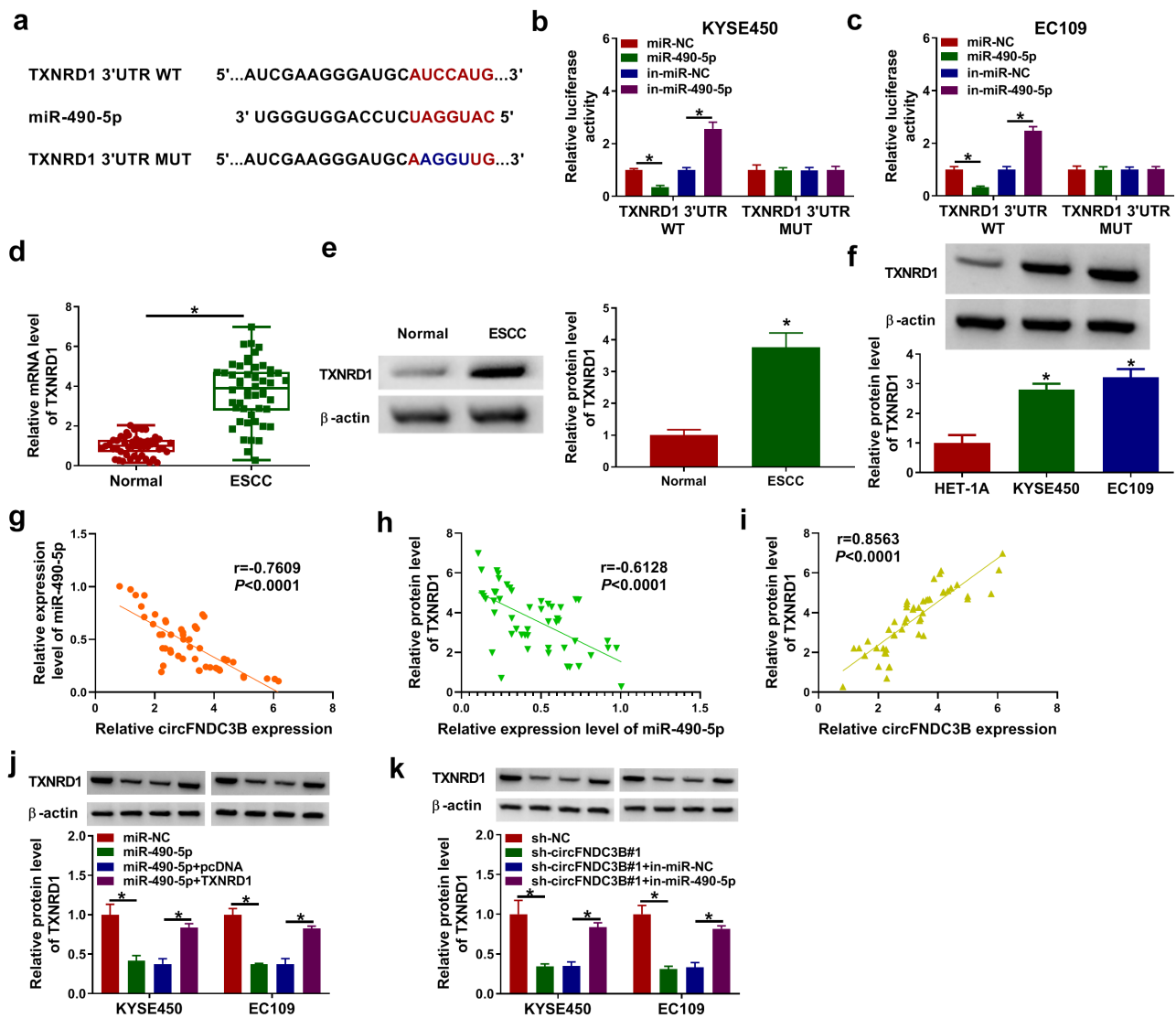


Figure 8. TXNRD1 was targeted by miR-490-5p. (a) Binding region between TXNRD1 and miR-490-5p and matched mutant sites were exhibited. (b,c) Dual-luciferase reporter assay was performed for verifying the targeting relationship between TXNRD1 and miR-490-5p (two-way ANOVA). (d) TXNRD1 mRNA level in normal and ESCC tissues was examined (Student's *t*-test). (e,f) TXNRD1 protein level was measured in normal tissues, ESCC tissues, HET-1A cells, and ESCC cells (KYSE450 and EC109) (Student's *t*-test and one-way ANOVA). (g-i) Pearson correlation coefficient assessed the correlation among miR-490-5p, circFNDC3B, and TXNRD1. (j) TXNRD1 protein level was tested in KYSE450 and EC109 cells transfected with miR-NC, miR-490-5p, miR-490-5p + pcDNA, or miR-490-5p + TXNRD1 (two-way ANOVA). (k) TXNRD1 protein expression was examined in KYSE450 and EC109 cells transfected with sh-NC, sh-circFNDC3B#1, sh-circFNDC3B#1 + in-miR-NC, or sh-circFNDC3B#1 + in-miR-490-5p (two-way ANOVA). * $P < 0.05$.

sponged by circFNDC3B. MiR-490-5p is able to function as an inhibitor in diverse tumors, including ESCC. For instance, miR-490-5p was downregulated in hepatocellular carcinoma and its upregulation suppressed the metastasis of hepatocellular carcinoma via downregulation of E2F2 and ECT2 [43]. In addition, miR-490-5p targeted PIK3CA to repress

tumor growth in renal cell carcinoma [44]. More importantly, miR-490-5p upregulation could suppress ESCC cell proliferation and invasion [44]. Herein, we found a decrease in miR-490-5p level in ESCC cell lines and tissue specimens. Furthermore, we found that Exo-sh-circFNDC3B#1 + in-miR-490-5p could reverse the biological role of Exo-sh-

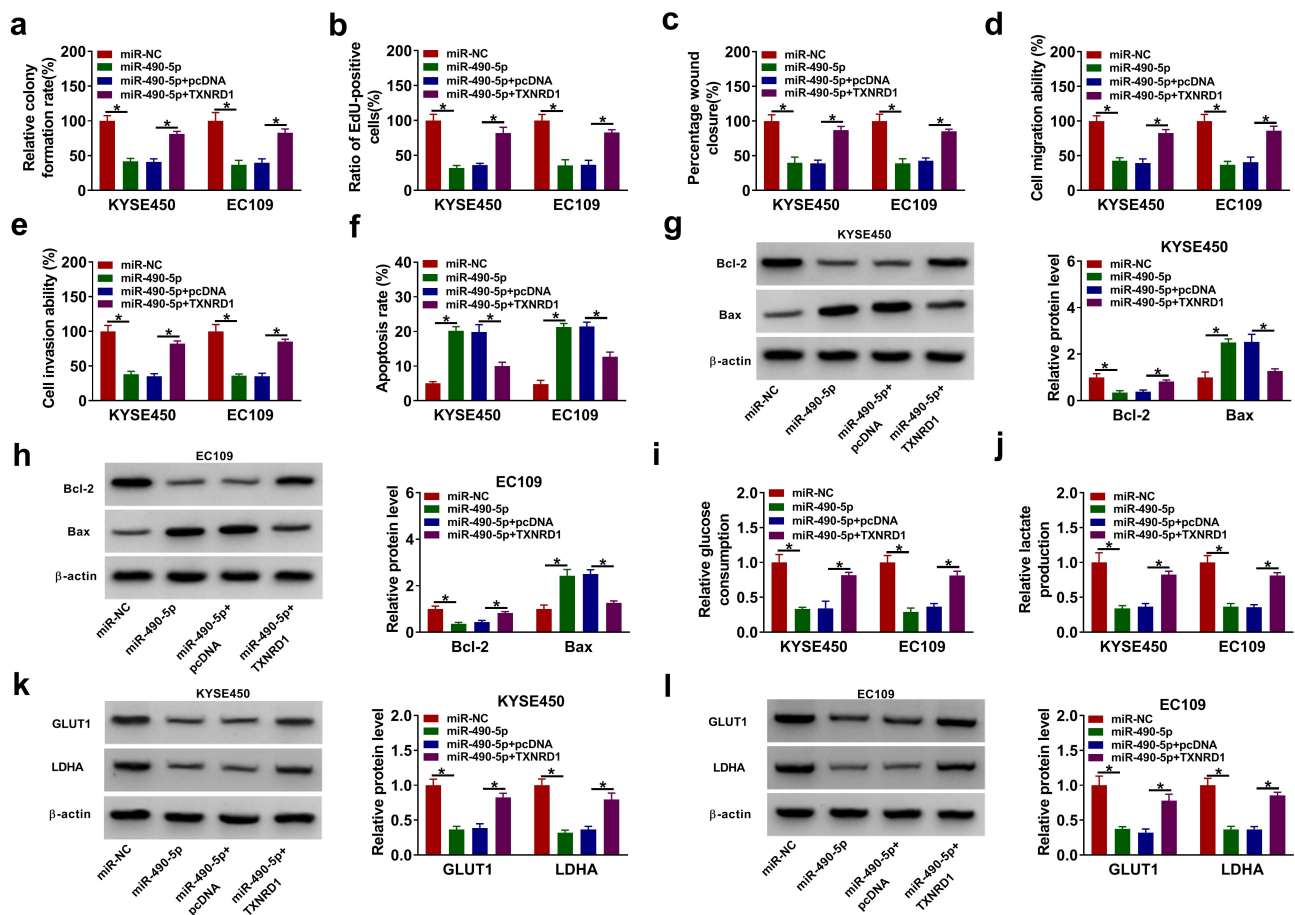


Figure 9. MiR-490-5p targeted TXNRD1 to exert the anti-tumor role in ESCC cells. KYSE450 and EC109 cells were transfected with miR-NC, miR-490-5p, miR-490-5p + pcDNA, or miR-490-5p + TXNRD1. (a,b) Cell proliferation was evaluated (two-way ANOVA). (c-e) Cell migratory and invasive abilities were determined (two-way ANOVA). (f) Cell apoptosis was detected (two-way ANOVA). (g,h) The expression levels of Bax and Bcl-2 were examined (two-way ANOVA). (i,j) Glucose consumption and lactate production were tested (two-way ANOVA). (k,l) GLUT1 and LDHA protein levels were analyzed (two-way ANOVA). * $P < 0.05$.

circFNDC3B#1 in recipient ESCC cells, indicating exosomal circFNDC3B exerted its role in ESCC cells through modulating miR-490-5p expression.

MiRNAs are able to bind with the 3'UTR of target mRNAs to affect the progression of cancer [45]. According to bioinformatics tool and experimental verification, we verified that TXNRD1 could directly bind to miR-490-5p. TXNRD1 is a key factor in regulating cell redox balance and plays a crucial role in protecting cells against oxidative stress [46]. Interestingly, TXNRD1 is overexpressed in multiple human malignancies and accelerates cancer progression [47,48]. Importantly, Li *et al.* disclosed that TXNRD1 was overexpressed in ESCC tissues, and miR-1305 exerted a tumor-suppressive function in ESCC cells via repressing

TXNRD1 [23]. Consistently, we found that TXNRD1 level was enhanced in ESCC, and TXNRD1 upregulation abated the repressive function of miR-490-5p by increasing cell growth, mobility and glycolysis and decreasing apoptosis in ESCC cells. *In vivo* experiments further confirmed that reducing exosome-shuttling circFNDC3B limited tumor growth *in vivo*.

Conclusion

In summary, our findings showed that decreasing exosomal circFNDC3B could inhibit ESCC progression by modulating the miR-490-5p/TXNRD1 axis. The study indicated that circFNDC3B might be

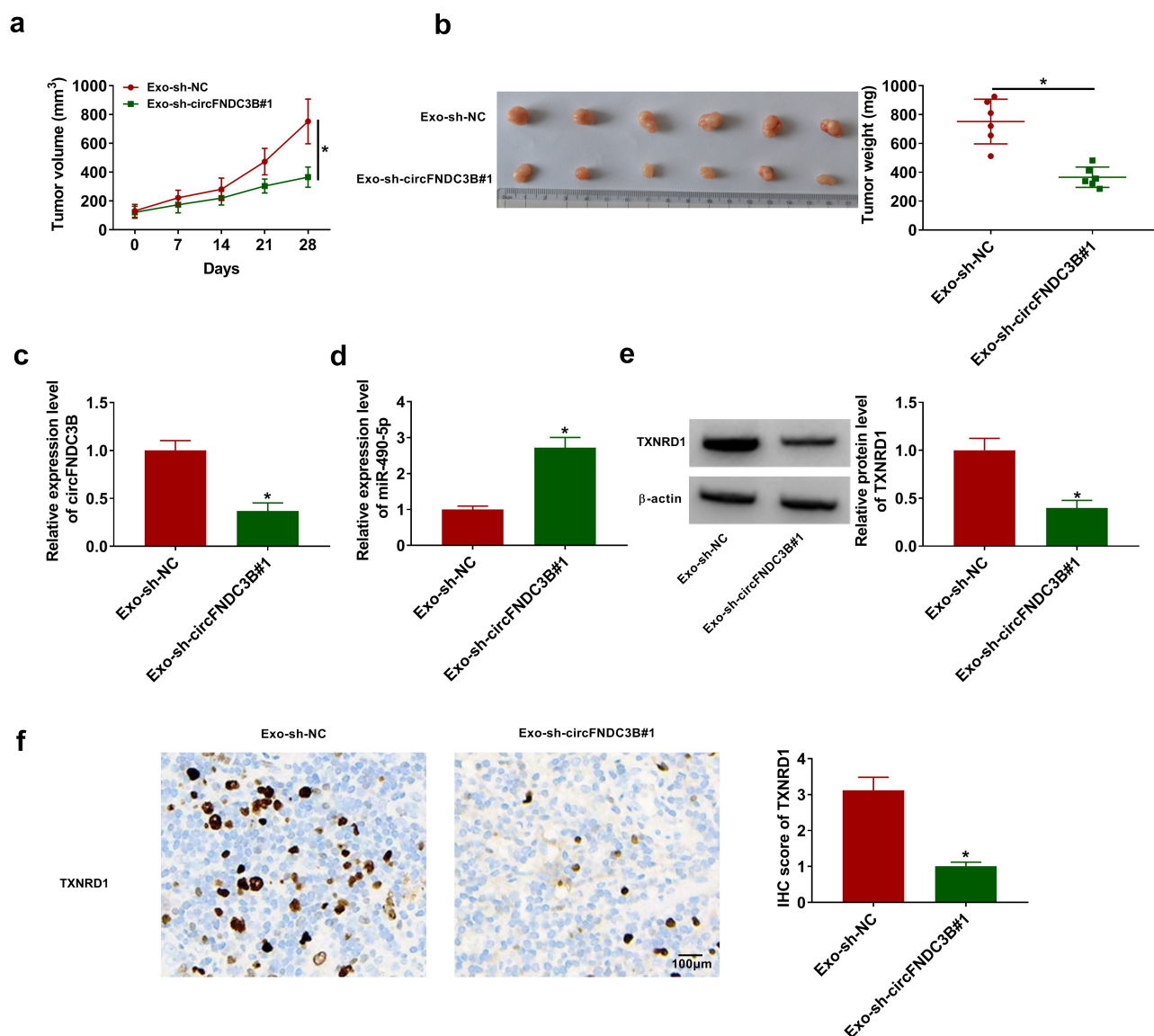


Figure 10. Reduction of exosomal circFND3B suppressed tumor growth *in vivo*. Donor EC109 cells introduced with sh-NC or sh-circFND3B#1 were co-cultured with recipient EC109 cells, and then recipient EC109 cells were introduced into nude mice for establishing mice xenograft model. (a,b) The volume (two-way ANOVA) and weight (Student's *t*-test) of tumors were measured. (c,d) CircFND3B and miR-490-5p expression levels in tumor tissues were determined (Student's *t*-test). (e) TXNRD1 protein expression was examined (Student's *t*-test). (f) TXNRD1 expression was tested using IHC analysis (Student's *t*-test). **P* < 0.05.

a possible biomarker for the diagnosis or treatment of ESCC.

Disclosure statement

No potential conflict of interest was reported by the author(s).

Funding

The author(s) reported there is no funding associated with the work featured in this article.

Ethical approval

All tissues samples were collected with written informed consent in accordance with the Declaration of Helsinki and with the approval of the Ethics Committee of Zigong Fourth People's Hospital.

Data availability statement

All data generated or analyzed during this study are included in this article.

References

- [1] Kelly RJ. Emerging multimodality approaches to treat localized esophageal cancer. *J Natl Compr Canc Netw*. 2019;17:1009–1014.
- [2] Watanabe M, Otake R, Kozuki R, et al. Recent progress in multidisciplinary treatment for patients with esophageal cancer. *Surg Today*. 2020;50:12–20.
- [3] Lin HN, Chen LQ, Shang QX, et al. A meta-analysis on surgery with or without postoperative radiotherapy to treat squamous cell esophageal carcinoma. *Int J Surg*. 2020;80:184–191.
- [4] Kato K, Cho BC, Takahashi M, et al. Nivolumab versus chemotherapy in patients with advanced oesophageal squamous cell carcinoma refractory or intolerant to previous chemotherapy (ATTRACTION-3): a multicentre, randomised, open-label, phase 3 trial. *Lancet Oncol*. 2019;20:1506–1517.
- [5] Yang H, Liu H, Chen Y, et al. Long-term efficacy of neoadjuvant chemoradiotherapy plus surgery for the treatment of locally advanced esophageal squamous cell carcinoma: the NEOCRTEC5010 randomized clinical trial. *JAMA Surg*. 2021;156:721–729.
- [6] Li X, Yang L, Chen LL. The biogenesis, functions, and challenges of circular RNAs. *Mol Cell*. 2018;71:428–442.
- [7] Chen LL, Yang L. Regulation of circRNA biogenesis. *RNA Biol*. 2015;12:381–388.
- [8] Wang Y, Mo Y, Gong Z, et al. Circular RNAs in human cancer. *Mol Cancer*. 2017;16:25.
- [9] Wang Y, Liu J, Ma J, et al. Exosomal circRNAs: biogenesis, effect and application in human diseases. *Mol Cancer*. 2019;18:116.
- [10] Cocucci E, Meldolesi J. Ectosomes and exosomes: shedding the confusion between extracellular vesicles. *Trends Cell Biol*. 2015;25:364–372.
- [11] Vlassov AV, Magdaleno S, Setterquist R, et al. Exosomes: current knowledge of their composition, biological functions, and diagnostic and therapeutic potentials. *Biochim Biophys Acta*. 2012;1820:940–948.
- [12] Ge R, Tan E, Sharghi-Namini S, et al. Exosomes in cancer microenvironment and beyond: have we overlooked these extracellular messengers? *Cancer Microenviron*. 2012;5(3):323–332.
- [13] Li Y, Feng W, Kong M, et al. Exosomal circRNAs: a new star in cancer. *Life Sci*. 2021;269:119039.
- [14] Pan Z, Lin J, Wu D, et al. Hsa_circ_0006948 enhances cancer progression and epithelial-mesenchymal transition through the miR-490-3p/HMGA2 axis in esophageal squamous cell carcinoma. *Aging (Albany NY)*. 2019;11:11937–11954.
- [15] Bach DH, Lee SK, Sood AK. Circular RNAs in cancer. *Mol Ther Nucleic Acids*. 2019;16:118–129.
- [16] Zhong Y, Du Y, Yang X, et al. Circular RNAs function as ceRNAs to regulate and control human cancer progression. *Mol Cancer*. 2018;17:79.
- [17] Ardekani AM, Naeini MM. The role of microRNAs in human diseases. *Avicenna J Med Biotechnol*. 2010;2:161–179.
- [18] Jansson MD, Lund AH. MicroRNA and cancer. *Mol Oncol*. 2012;6:590–610.
- [19] Sun Y, Qiu L, Chen J, et al. Construction of circRNA-Associated ceRNA network reveals novel biomarkers for esophageal cancer. *Comput Math Methods Med*. 2020;2020:7958362.
- [20] Zhou PL, Wu Z, Zhang W, et al. Circular RNA hsa_circ_0000277 sequesters miR-4766-5p to upregulate LAMA1 and promote esophageal carcinoma progression. *Cell Death Dis*. 2021;12:676.
- [21] Chen X, Jiang J, Zhao Y, et al. Circular RNA circNTRK2 facilitates the progression of esophageal squamous cell carcinoma through up-regulating NR1P1 expression via miR-140-3p. *J Exp Clin Cancer Res*. 2020;39:133.
- [22] Li FZ, Zang WQ. Knockdown of lncRNAXLOC_001659 inhibits proliferation and invasion of esophageal squamous cell carcinoma cells. *World J Gastroenterol*. 2019;25:6299–6310.
- [23] Li X, Song L, Wang B, et al. Circ0120816 acts as an oncogene of esophageal squamous cell carcinoma by inhibiting miR-1305 and releasing TXNRD1. *Cancer Cell Int*. 2020;20:526.
- [24] Livak KJ, Schmittgen TD. Analysis of relative gene expression data using real-time quantitative PCR and the 2^{(-delta delta C(T))} method. *Methods*. 2001;25:402–408.
- [25] Guo X, Zhu R, Luo A, et al. EIF3H promotes aggressiveness of esophageal squamous cell carcinoma by modulating snail stability. *J Exp Clin Cancer Res*. 2020;39:175.
- [26] Cao S, Chen G, Yan L, et al. Contribution of dysregulated circRNA_100876 to proliferation and metastasis of esophageal squamous cell carcinoma. *Onco Targets Ther*. 2018;11:7385–7394.
- [27] Chen L, Pan J. Dual cyclin-dependent kinase 4/6 inhibition by PD-0332991 induces apoptosis and senescence in oesophageal squamous cell carcinoma cells. *Br J Pharmacol*. 2017;174:2427–2443.
- [28] Chen YH, Lu HI, Lo CM, et al. CD73 promotes tumor progression in patients with esophageal squamous cell carcinoma. *Cancers (Basel)*. 2021;13:3982.
- [29] Mai S, Liu L, Jiang J, et al. Oesophageal squamous cell carcinoma-associated IL-33 rewires macrophage polarization towards M2 via activating ornithine decarboxylase. *Cell Prolif*. 2021;54:e12960.
- [30] Kang JY, Park H, Kim H, et al. Human peripheral blood-derived exosomes for microRNA delivery. *Int J Mol Med*. 2019;43:2319–2328.
- [31] Zhang H, Zhu L, Bai M, et al. Exosomal circRNA derived from gastric tumor promotes white adipose browning by targeting the miR-133/PRDM16 pathway. *Int J Cancer*. 2019;144:2501–2515.

- [32] Li Z, Qin X, Bian W, et al. Exosomal lncRNA ZFAS1 regulates esophageal squamous cell carcinoma cell proliferation, invasion, migration and apoptosis via microRNA-124/STAT3 axis. *J Exp Clin Cancer Res.* **2019**;38:477.
- [33] Dong W, Bi J, Liu H, et al. Circular RNA ACVR2A suppresses bladder cancer cells proliferation and metastasis through miR-626/EYA4 axis. *Mol Cancer.* **2019**;18:95.
- [34] Wu Z, Wu J, Zhao Q, et al. Emerging roles of aerobic glycolysis in breast cancer. *Clin Transl Oncol.* **2020**;22:631–646.
- [35] Alsop BR, Sharma P. Esophageal cancer. *Gastroenterol Clin North Am.* **2016**;45:399–412.
- [36] Takahashi K, Yan IK, Kogure T, et al. Extracellular vesicle-mediated transfer of long non-coding RNA ROR modulates chemosensitivity in human hepatocellular cancer. *FEBS Open Bio.* **2014**;4:458–467.
- [37] Li Y, Zang H, Zhang X, et al. Exosomal Circ-ZNF652 promotes cell proliferation, migration, invasion and glycolysis in hepatocellular carcinoma via miR-29a-3p/GUCD1 axis. *Cancer Manag Res.* **2020**;12:7739–7751.
- [38] Xie M, Yu T, Jing X, et al. Exosomal circSHKBP1 promotes gastric cancer progression via regulating the miR-582-3p/HUR/VEGF axis and suppressing HSP90 degradation. *Mol Cancer.* **2020**;19:112.
- [39] Liu F, Wang N, Wei J, et al. Circ_0006948 drives the malignant development of bladder cancer via activating the epithelial-mesenchymal transition. *J BUON.* **2021**;26:1491–1497.
- [40] Yue M, Liu Y, Zuo T, et al. Circ_0006948 contributes to cell growth, migration, invasion and epithelial-mesenchymal transition in esophageal carcinoma. *Dig Dis Sci.* **2022**;67:492–503.
- [41] Tang R, Zhou Q, Xu Q, et al. Circular RNA circ_0006948 promotes esophageal squamous cell carcinoma progression by regulating microRNA-3612/LASP1 axis. *Dig Dis Sci.* **2021**. DOI:10.1007/s10620-021-07057-4.
- [42] Greene J, Baird AM, Brady L, et al. Circular RNAs: biogenesis, function and role in human diseases. *Front Mol Biosci.* **2017**;4:38.
- [43] Fang ZQ, Li MC, Zhang YQ, et al. MiR-490-5p inhibits the metastasis of hepatocellular carcinoma by down-regulating E2F2 and ECT2. *J Cell Biochem.* **2018**;119:8317–8324.
- [44] Chen K, Zeng J, Tang K, et al. miR-490-5p suppresses tumour growth in renal cell carcinoma through targeting PIK3CA. *Biol Cell.* **2016**;108:41–50.
- [45] Vishnoi A, Rani S. MiRNA biogenesis and regulation of diseases: an overview. *Methods Mol Biol.* **2017**;1509:1–10.
- [46] Arnér ES. Focus on mammalian thioredoxin reductases—important selenoproteins with versatile functions. *Biochim Biophys Acta.* **2009**;1790:495–526.
- [47] Hua S, Quan Y, Zhan M, et al. miR-125b-5p inhibits cell proliferation, migration, and invasion in hepatocellular carcinoma via targeting TXNRD1. *Cancer Cell Int.* **2019**;19:203.
- [48] Hao C, Xu X, Ma J, et al. MicroRNA-124 regulates the radiosensitivity of non-small cell lung cancer cells by targeting TXNRD1. *Oncol Lett.* **2017**;13:2071–2078.